J Appl Electrochem (2009) 39:2337–2344
DOI 10.1007/s10800-009-9918-y

ORIGINAL PAPER

# Copper–nickel codeposition as a model for mass-transfer characterization in copper–indium–selenium thin-film production

**A. Ollivier · L. Muhr · S. Delbos · P. P. Grand · M. Matlosz · E. Chassaing**

Received: 21 November 2008 / Accepted: 27 April 2009 / Published online: 9 May 2009


**Abstract** The use of binary copper–nickel (Cu–Ni) codeposition from a complexing citrate electrolyte is proposed as a convenient model system for simple, rapid and inexpensive characterization of local mass-transfer limitations arising in the production of ternary copper-indium-selenium (CIS) thin films. Both the Cu–Ni and the CIS systems have been investigated in a small pilot cell and deposit thickness and composition distributions on a $5 \times 5$ cm$^2$ cathode have been compared. The experimental comparison confirms that the mass-transfer characteristics measured for copper deposition in the binary Cu–Ni codeposition system offer an excellent representation of the mass-transfer-limited deposition of copper and selenium in the ternary CIS system. The binary Cu–Ni system presents a number of advantages for process development, among which the possibility of operating at neutral pH and being much easier to handle, less expensive and less toxic than the CIS system. The results of the study presented here, although targeted to CIS production, may also be of use for the development of other electrodeposition processes in which one or more electro-active species are reduced under mass-transfer control.

A. Ollivier · S. Delbos · P. P. Grand · E. Chassaing
Institute of R&D on Photovoltaic Energy,
UMR 7174, EDF-CNRS-ENSCP, 6, quai Watier,
78401 Chatou Cedex, France

A. Ollivier · L. Muhr (✉) · M. Matlosz
Laboratoire des Sciences du Génie Chimique, Nancy-Université,
CNRS, ENSIC, LSGC, 1, rue Grandville, BP 20451,
54001 Nancy, France
e-mail: Laurence.Muhr@ensic.inpl-nancy.fr

**Keywords** Alloy electrodeposition · Mass-transfer · Hydrodynamics · Process scale-up

## 1 Introduction

Recent development efforts on innovative thin-layer solar cells have been focused on absorber layers composed of $CuInSe_2$ (CIS) thin films electrodeposited onto molybdenum-coated glass substrates [1, 2]. For the application to be effective, both the thickness and the composition of the deposited thin films must be uniform over the entire substrate area, and this has been achieved for small surfaces under well-controlled hydrodynamic conditions. Scale-up of the process to much larger surface areas, however, can lead to undesirable non-uniform composition and thickness distributions, and extensive investigation of hydrodynamic conditions is therefore essential for industrial process design [3].

Since the pioneering work of Bhattacharya [4], electrodeposition of CIS has been extensively investigated by numerous authors [5–12]. The ternary system is complex, however, and several issues concerning the deposition mechanism still remain unresolved [13].

Since the standard redox potential for indium ($E^\circ$ for In(III)/In $= -0.348$ V/NHE) in aqueous solution is much lower than that of copper ($E^\circ$ for Cu(II)/Cu $= +0.335$ V/NHE) and of selenium ($E^\circ$ for $H_2SeO_3$/Se $= +0.739$ V/NHE), it can be expected that deposition of the ternary alloy CIS will occur at relatively negative potentials, with deposition of selenium and copper occurring under mass-transfer control and indium under charge-transfer control. This hypothesis is supported by experimental observations showing that the Se/Cu ratio in the electrodeposited thin-layer CIS films is directly proportional to the ratio of the mass-transfer rates for Se(IV) and Cu(II) in solution [7].

The incorporation mechanism of indium in the electrodeposit has been a matter of discussion [12]. It appears that interactions with the Cu-Se phase result in indium deposition at a potential more positive than its equilibrium value, thereby suggesting a mechanism similar to that proposed by Kröger for CdTe deposition [14]. Due to the interactions, indium deposition is not under pure charge-transfer control. Nevertheless, the indium content in the CIS layer does depend on electrode potential and can be represented by quasi-Tafel behavior with a low activation constant [13].

The chemistry of selenium in aqueous solution is complex, since the element can exhibit up to four different oxidation states : −2, 0, +4 and +6. In CIS thin-film production, in addition to the majority phase composed of $CuInSe_2$, analysis of the electrodeposits reveals the presence of smaller quantities of two other phases: a Cu–Se phase and a phase of elemental Se [10, 15].

The solubility of the In(III) species in aqueous solutions is extremely limited, and particularly low at neutral pH. Consequently, effective electrolytes for CIS thin-film production require either very high or very low pH [16]. In industrial practice, typical electrolytes are generally acid solutions containing relatively low concentrations of indium, copper and selenium. Mass-transfer limitations for copper and selenium are therefore unavoidable, and the performance of electrodeposition processes for thin-film production is largely influenced by hydrodynamic conditions.

For large-scale applications, accurate knowledge of local mass transfer and hydrodynamics is essential for design of process conditions that ensure uniform film thickness and composition, and obtaining such knowledge under the complex hydrodynamic conditions encountered in industrial practice requires substantial experimental study. Unfortunately, the cost and toxicity of electrolyte solutions containing indium and selenium salts renders their use particularly inconvenient for direct experimentation on the laboratory and pilot-plant scales during the initial phases of process development.

The objective of the present study is therefore focused on the question of simple, rapid and accurate characterization of hydrodynamic conditions and local mass transfer for electrodeposition of copper and selenium in CIS thin-film production. The more complex issue of the precise charge-transfer mechanism for incorporation of indium in the ternary deposits is not directly addressed.

The binary codeposition system proposed in this work for mass-transfer characterization is copper–nickel codeposition from a complexing citrate electrolyte. The binary Cu–Ni system, if representative as a model for mass-transfer, should offer numerous advantages, among which the possibility of operating at neutral pH and being much easier to handle, less expensive and less toxic than direct experimentation with CIS.

## 2 Cu–Ni electrodeposition as a model system for mass-transfer characterization

An effective model tracer system for characterization of mass-transfer and hydrodynamics in an electrodeposition process should possess the following features :

- a binary electrolyte system, with one (minority) species depositing under complete mass-transfer control and the other (majority) species under complete charge-transfer control
- a sufficiently wide range of mass-transfer rates over a substantial potential range with high current efficiency (absence of significant hydrogen evolution that could influence local hydrodynamics)
- smooth (dendrite-free) deposits over the complete composition range of electrodeposits produced
- a simple and reliable method for local measurement of deposit thickness and deposit composition (including non-destructive mapping of thickness and composition as a function of position over the electroplated surface)

The essential features of partial-current polarization behavior expected to satisfy the requirements outlined above are shown schematically in Fig. 1 [17]. Although several electrolyte systems may be potential candidates, Cu–Ni codeposition from complexing citrate electrolytes is an attractive choice for the present study. Mass-transfer-controlled copper deposition with charge-transfer-controlled nickel deposition over a wide potential range with high current efficiency is possible, the complexing citrate baths offer the advantage of particularly smooth, dendrite-free, low-roughness deposits, and measurement of electrodeposit

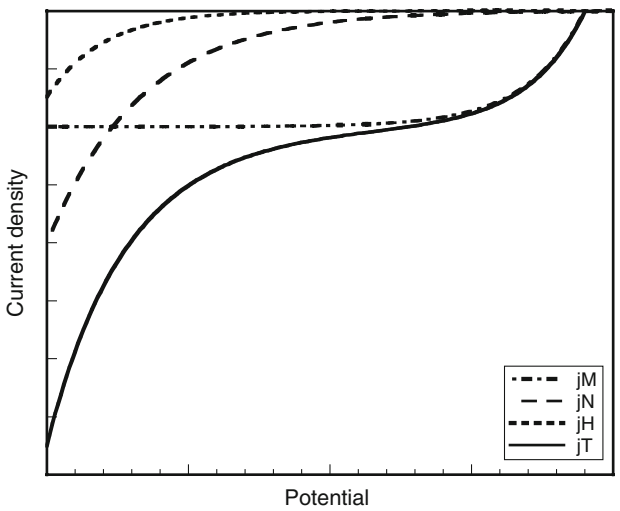


**Fig. 1** Schematic representation of polarization curves, $j_M$ and $j_N$, for M, N partial deposition current density, $j_H$, for hydrogen evolution and $j_T$ the total deposition current density during the codeposition of M-N

thickness and copper and nickel composition by X-ray fluorescence is available for non-destructive mapping. The Cu–Ni-citrate electrolyte offers the additional advantages of ease of preparation and handling, low cost and operation at neutral pH.

The Cu–Ni codeposition system is well known and has been frequently employed for the production of protective coatings [18–24]. Electrodeposited Monel alloys, for example, containing 70% nickel, are widely used for their excellent corrosion resistance in naval installations [18]. Although the electrodeposition of compact, non-dendritic Cu–Ni alloys is not possible from plating baths of simple mineral salts, high-quality deposits from baths containing complexing agents can be easily obtained [18]. Citric acid or trisodium citrate are attractive complexing agents for this purpose, since they are effective, inexpensive and non-toxic [19]. In the presence of citrate, the deposition potentials for Cu and Ni are closer, but Cu nevertheless remains substantially nobler. As a result, Cu is typically discharged under mass-transfer control, whereas nickel remains under charge-transfer control over a significant potential range [20–22]. Copper and nickel form a continuous solid solution and Cu–Ni deposits from citrate electrolytes are single-phase alloys.

## 3 Experimental

The electrodeposition investigations for Cu–Ni codeposition have been performed in three-electrode cells, with two different electrolyte compositions typical of Priscott baths [19]. The composition of the two electrolyte solutions is shown in Table 1. The plating baths are aqueous solutions prepared with copper and nickel sulfate and trisodium citrate. A saturated mercury/mercurous sulfate reference (MSE) is employed for potential measurement (MSE, $E = +0.65$ V/NHE).

Substrates for electrodeposit are 2–3 mm thick glass plates coated with a DC-magnetron-sputtered layer of molybdenum (Mo thickness of 500–600 nm), provided by Saint Gobain Recherche [1, 2]. The substrates are cleaned in concentrated ammonia solution prior to each experiment and rinsed under flowing high-purity water.

A rotating disk electrode has been used to investigate the deposition kinetics of the systems. The electrolyte volume is 500 mL, with a working electrode area of 0.785 $cm^2$. Rotation speeds are varied from 100 to 3,000 rpm. The counter-electrode is a platinum coil.

Larger-scale experiments have been carried out in a small pilot unit, composed of a vertical cell with parallel $5 \times 5$ $cm^2$ electrodes. The cell volume is 1,000 mL, with agitation provided by a comb-like system [3]. An Autolab or Biologic VMP3 potentiostat/galvanostat is employed as a current supply, with voltammetric investigation carried out to determine the available potential domain for electrodeposition.

The equivalent thickness and composition of the Cu–Ni films are determined by X-ray fluorescence (Fischerscope X-Ray Xan). The deposited mass is calculated using a density value of 8.9 g $cm^{-3}$, similar to the densities of elemental nickel and copper. Partial current densities for copper and nickel deposition are calculated according to Faraday's law. Flow-field velocities are measured by Laser Doppler Velocimetry (LDV).

## 4 Rotating disk measurements

### 4.1 Voltammetric investigation of the Cu–Ni system

Figure 2 shows polarization curves recorded at 200 and 500 rpm for each of the two Cu–Ni plating baths. Three main potential domains are visible [23]. At low overpotentials, the magnitude of the current density increases with increasing negative (cathodic) polarization. In the potential range from −0.8 to −1.5 V/MSE, a pseudo-plateau is observed whose magnitude is proportional to the cupric-ion concentration in solution. For more negative potentials, hydrogen evolution is observed resulting from solvent reduction.

Between −1.0 and −1.5 V/MSE, the magnitude of the current density increases with electrode rotation speed. Figure 3 shows the results for the higher cupric-ion concentration (electrolyte no. 2 in Table 1). The variation of reciprocal current density as a function of the reciprocal square root of the electrode rotation speed is plotted at various electrode potentials. For potentials lower than −1.5 V/MSE, no significant increase in the magnitude of the reduction current is observed since solvent reduction resulting in hydrogen evolution is the main reaction. In the potential range from −1.0 to −1.5 V/MSE, Koutecky–Levich behavior is observed:

**Table 1** Composition of the Cu–Ni solutions (mol $L^{-1}$)

| | $CuSO_4$, $5H_2O$ (mol $L^{-1}$) | $NiSO_4$, $7H_2O$ (mol $L^{-1}$) | $Na_3Cit$, $2H_2O$ (mol $L^{-1}$) |
|---|---|---|---|
| Electrolyte 1 | 0.0095 | 0.185 | 0.25 |
| Electrolyte 2 | 0.0250 | 0.165 | 0.25 |

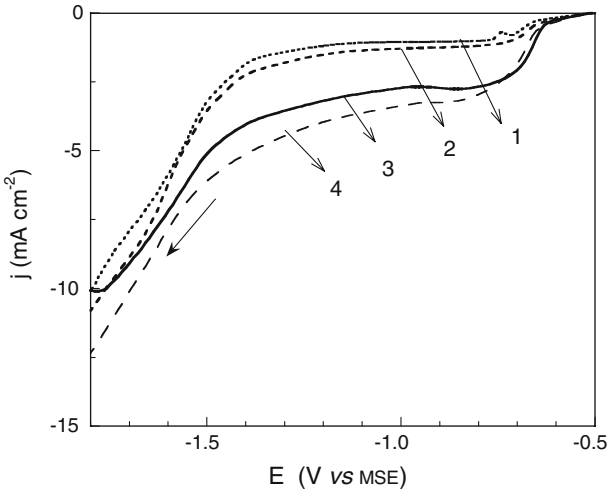


**Fig. 2** Cathodic polarization curves recorded at 10 mV $s^{-1}$. *Curve 1*: Electrolyte 1, electrode rotation rate: 200 rpm, *Curve 2*: Electrolyte 1, electrode rotation rate: 500 rpm, *Curve 3*: Electrolyte 2, electrode rotation rate: 200 rpm, *Curve 4*: Electrolyte 2, electrode rotation rate: 500 rpm

$$\frac{1}{j} = \frac{1}{j_k} + \frac{1}{B\omega^{1/2}} \quad (1)$$

where $j_k$ denotes the charge-transfer rate in the absence of mass-transfer limitation and $B\omega^{1/2}$ is a mass-transfer rate where the parameter B is defined for a rotating disk as follows:

$$B = 0.62\ n\ F\ D^{2/3} v^{-1/6} C_b \quad (2)$$

In this potential range, copper deposition is largely mass-transfer controlled.

The experimental value of B of 1.15 ± 0.05 mA $cm^{-2}$ $rd^{-1/2}$ $s^{1/2}$ is in good agreement with the estimate of 1.24 mA $cm^{-2}$ $rd^{-1/2}$ $s^{1/2}$ obtained from Eq. 2 for a diffusion coefficient of cupric species of 3 × $10^{-6}$ $cm^2$ $s^{-1}$ and a kinematic viscosity of 1.6 × $10^{-2}$ $cm^2$ $s^{-1}$ [21]. The intercept, $1/j_k$, varies exponentially with potential, corresponding to expected Tafel behavior for the charge-transfer kinetics of nickel deposition.

### 4.2 Steady-state investigation

For determination of the steady-state polarization behaviour, the most concentrated solution (No. 2 in Table 1) has been employed in order to limit the effect of cupric ion depletion during long time deposition. Several deposits were produced at various potentials for an electrode rotation speed of 100 rpm. The partial-current polarization curves, calculated using Faraday's law, are shown in Fig. 4 together with the total polarization curve. The partial-current curve for copper deposition (curve 2) shows a nearly constant current density of 2.3 ± 0.3 mA $cm^{-2}$, thereby confirming that copper is deposited under mass-transfer control. As already observed, nickel begins to codeposit beyond a certain potential threshold, close to –1.3 V (curve 3). In the potential range from –1.3 to –1.55 V, the nickel partial current shows a quasi-exponential behaviour. At potentials more negative than –1.55 V, the Ni–Cu films exhibit high tensile stresses, most likely due to increased hydrogen evolution. As a result, they tend to peel away from the electrode surface for low deposit thicknesses.

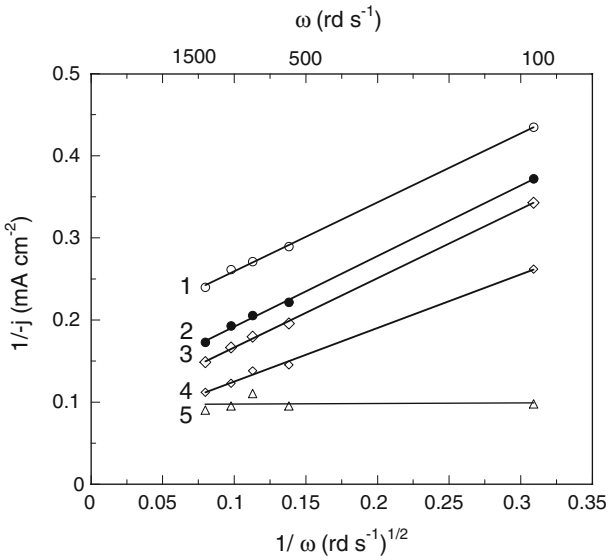


**Fig. 3** Koutecky–Levich plot recorded in Cu–Ni electrolyte 2 for different deposition potentials: *Curve 1*: −1.0 V/MSE, *Curve 2*: −1.2 V/MSE, *Curve 3*: −1.3 V/MSE, *Curve 4*: −1.5 V/MSE, *Curve 5*: −1.6 V/MSE

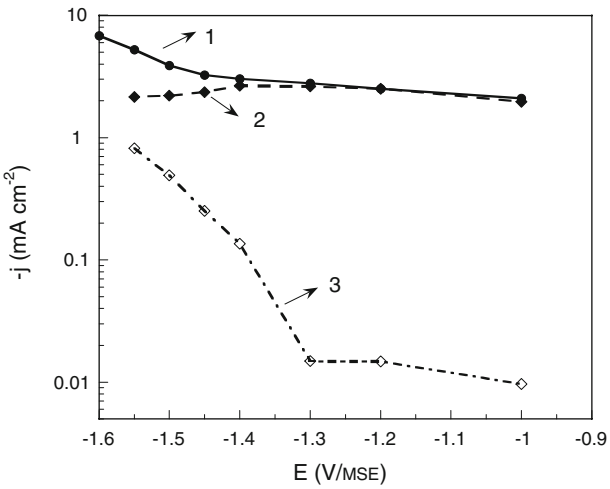


**Fig. 4** Steady-state polarization curves recorded in Cu–Ni electrolyte 2, disk electrode rotating at 100 rpm. *curve 1*: total polarization curve, *curve 2*: partial polarization curve for copper deposition, *curve 3*: partial polarization curve for nickel deposition

### 4.3 Voltammetric investigation of the Cu–In–Se electrodeposition system

Cu–In–Se films were electrodeposited from low concentration, i.e. millimolar, acidic solutions [1, 2]. Figure 5 shows the cathodic polarization curves for Cu–In–Se electrodeposition recorded at various electrode rotation speeds. With increasing cathodic overvoltage, the magnitude of the current increases and exhibits a maximum. Between –0.8 and –1.0 V, a current density plateau is observed, whose magnitude depends on the hydrodynamic conditions. In this potential range, the current density follows Koutecky–Levich behaviour as a function of the electrode rotation rate, as for the Cu–Ni system. It has been shown that copper and selenium are deposited under mass-transfer control [7, 8]. The value of coefficient B is equal to $0.5 \pm 0.1$ mA $cm^{-2}$ $rd^{-1/2}$ $s^{1/2}$, in reasonable agreement with the estimation of 0.48 mA $cm^{-2}$ $rd^{-1/2}$ $s^{1/2}$, based on values of diffusion coefficients for Cu and Se species of $D_{Cu} = 8.10^{-6}$ $cm^2$ $s^{-1}$ and $D_{Se} = 9.10^{-6}$ $cm^2$ $s^{-1}$, and a value of 0.01 $cm^2$ $s^{-1}$ for the kinematic viscosity. Similarly to the Cu–Ni system, a positive intercept is observed in the Koutecky–Levich plot for CIS (Fig. 6). The intercept is related to indium discharge, but is less strongly dependent on potential in comparison to the Cu–Ni system.

### 4.4 Potential dependence of the deposit composition

Figure 7 shows the Se/Cu and In/Cu ratio as a function of deposition potential. Three major potential domains can be identified [13]. At low overpotentials (domain (A)), binary Cu–Se compounds are deposited, with the Se content increasing with cathodic overpotential. As for nickel in the case of the Cu–Ni system, there exists a potential threshold beyond which indium is deposited (domain (B)). For potentials positive of –0.6 V, no indium is observed in the layer. For potentials negative of –0.6 V the indium content increases quasi-exponentially with increasing cathodic deposition potential. In the potential range of domain (C) (−0.8 V, −1.0 V) where the CIS layers are generally deposited in practice [1, 2], the indium content increases more slowly with overpotential.

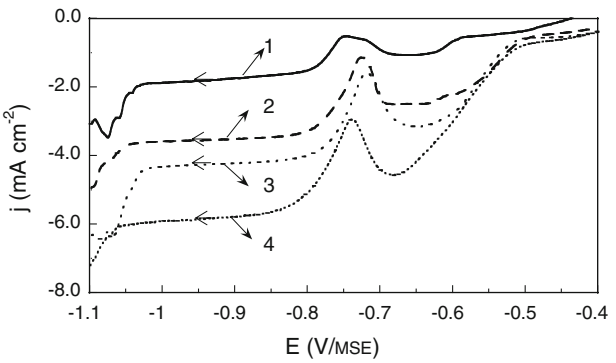


**Fig. 5** Cathodic polarization curves for Cu–In–Se deposition for different rotation rates. *Curve 1*: 100 rpm, *Curve 2*: 500 rpm, *Curve 3*: 750 rpm, *Curve 4*: 1,500 rpm

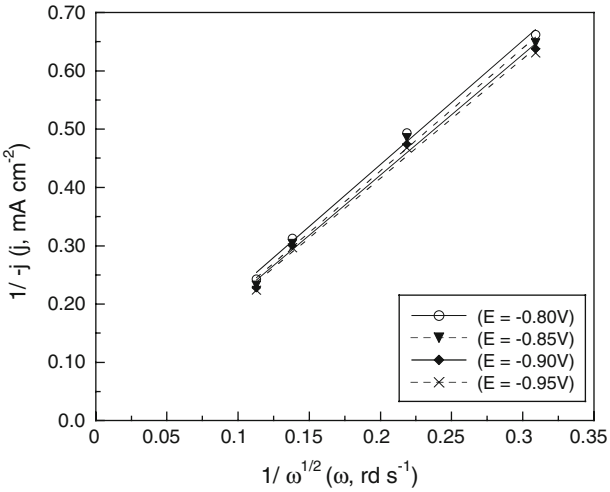


**Fig. 6** Koutecky–Levich plot recorded in Cu–In–Se electrolyte for different deposition potentials (−0.80 V, −0.85 V, −0.90 V and −0.95 V/MSE)

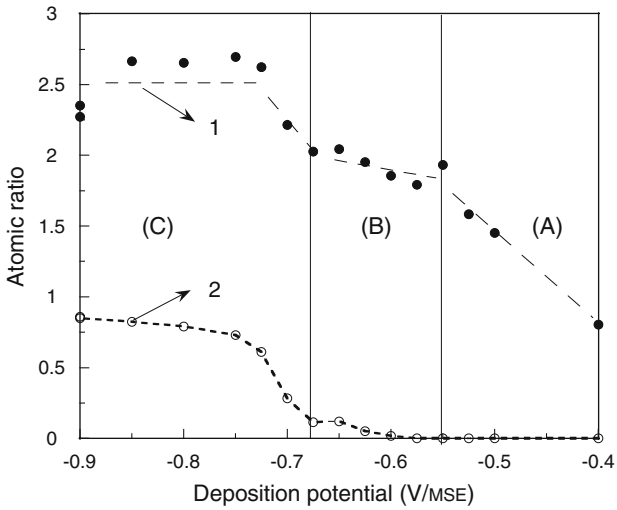


**Fig. 7** Se/Cu atomic ratio (*curve 1*) and In/Cu atomic ratio (*curve 2*) as a function of the deposition potential. Electrode rotation speed: 100 rpm

## 5 Pilot investigation: comparison between Cu–Ni and Cu–In–Se deposition

Several experiments were performed in the pilot cell under varying hydrodynamic conditions (comb velocity, tooth shape, etc.). The chemical composition and equivalent

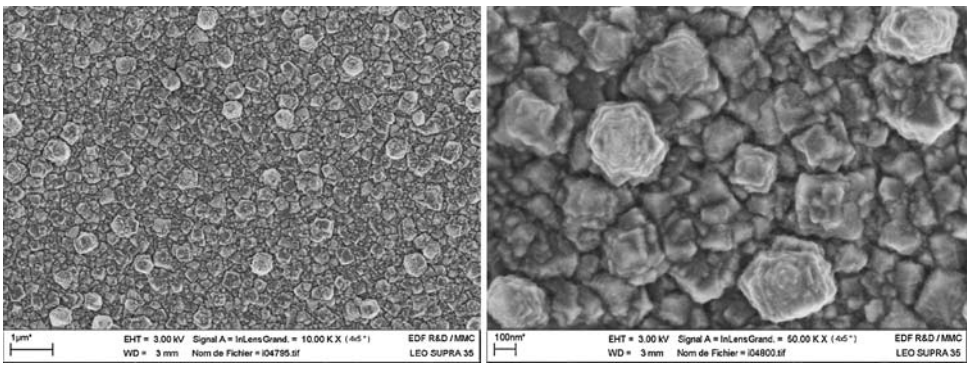

**Fig. 8** Surface morphology of a Cu–Ni film deposited at –1.6 V from electrolyte 2, thickness 0.7 μm, composition: 85% Cu, 15% Ni. **a** magnification 10,000, **b** magnification 50,000

thickness of the deposits were analysed locally using X-Ray Fluorescence, and the partial currents of copper and nickel were calculated using Faraday's law. The morphology of the deposited films shows nodules as often observed when the deposition process is controlled by mass transfer (Fig. 8 a and b).

Figure 9 shows an example of the distributions of the partial currents along horizontal lines on the cathode, for an experiment carried out at a deposition potential of –1.6 V/MSE and for a comb speed of 124 mm $s^{-1}$, corresponding to a stirring frequency of 5 Hz. The nickel partial current is nearly constant in the middle of the cathode and increases markedly on the edges, whereas the copper partial current exhibits oscillations along the cathode. These observations suggest differences in the relative importance of mass transfer and charge transfer for each of the two metals.

The current distribution for electrochemical deposition of binary alloys is generally divided into three contributions: primary, secondary or tertiary [17, 24, 25]. The primary distribution depends mainly on the geometry of the cell and results in increased current lines concentrated on the edges of the cathode [24], as observed in Fig. 9 for the partial current of nickel.

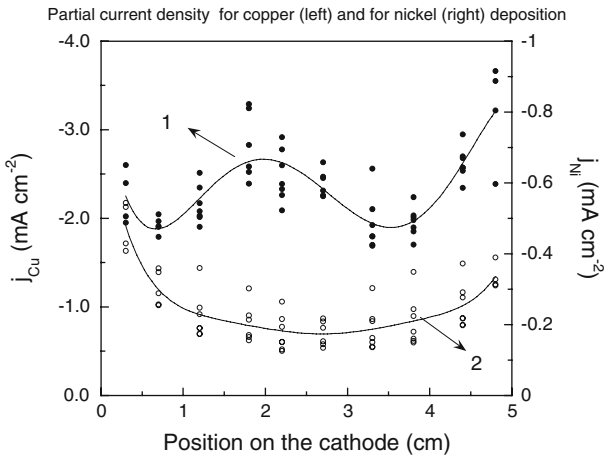


**Fig. 9** Current density distribution curves recorded along the cathode for a Cu–Ni layer deposited at −1.6 V/MSE from electrolyte 2. *Curve 1*: partial current for Cu and *curve 2* for Ni deposition (comb speed 124 mm $s^{-1}$, 5 Hz)

The secondary current distribution depends on the kinetics of the electrodeposition reactions and the importance of this distribution relative to the primary distribution can be expressed with a dimensionless parameter, the Wagner number, $W_a$, representing the ratio between the polarization resistance, $d\eta/dj$, at the deposition potential and the electrolyte resistance

$$W_a = \frac{\kappa}{L}\frac{d\eta}{dj}, \tag{3}$$

where $L$ is a characteristic length in the system and $\kappa$ the conductivity of the solution.

For sufficiently large overvoltage, Tafel approximation can be applied and the Wagner number can be expressed as follows:

$$W_a = \frac{\kappa}{L}\frac{\beta_c}{|j_{average}|} \tag{4}$$

where $\beta_c$ is the Tafel coefficient of the cathodic polarization curve. The higher the value of $W_a$, the more uniform the current distribution.

The tertiary current distribution depends on mass transfer conditions. Local variations in current density result from local variations in the thickness of the diffusion layer, $\delta$, which depends on local hydrodynamics.

At the limiting current density, the surface concentration of the electroactive species tends toward zero, and the tertiary current distribution predominates. Depending on the agitation mode, the value of $\delta$ may vary locally, as a function of both the horizontal and vertical positions, leading to local variation of the current density and of the film composition and thickness.

Figure 9 shows that the partial-current curve for copper deposition presents such fluctuations dependent on local hydrodynamics. This behaviour can be expected, since it has been shown that copper is deposited under mass-

transfer control. Both deposit thickness and copper content exhibit similar fluctuations, resulting from variations in the diffusion-layer thickness along the electrode surface.

By contrast, the nickel partial current is independent of hydrodynamic fluctuations, since nickel is deposited under charge-transfer control. In order to quantify the relative influence of primary and secondary current distribution effects, a Wagner number has been calculated. The $\beta_c$ coefficient, determined from a polarization curve carried out under the same experimental conditions (electrolyte 2, comb speed 124 mm $s^{-1}$) is found to be 100 mV. The conductivity of the solution was determined by impedance spectroscopy measurements as 0.025 $\Omega^{-1}$ $cm^{-1}$. The average current density at a deposition potential of –1.6 V is equal to 3.7 mA $cm^{-2}$.

The choice of characteristic length as the distance between the comb and the electrode (L = 0.8 cm) results in a Wagner number $W_a = 0.85$, a relatively low value.

Considering this Wagner number, it is to be expected that polarization resistance will not be preponderant in comparison to electrolyte resistance. Primary current distribution effects are therefore likely resulting in a substantial increase in local current density at the electrode edges, as effectively observed in Fig. 9 for nickel.

Similar experiments have been carried out for CIS deposition in the pilot cell. Curve 1 in Fig. 10 shows the flow field distribution on the cathode for a comb speed of 104 mm $s^{-1}$ as measured by Laser Doppler Velocimetry (LDV). The mean velocity presents periodic fluctuations along the cathode, and the ratio of local versus average thickness, plotted together for CIS (curve 2) and Cu–Ni (curve 3) along the cathode, shows that the local thickness follows closely the local flow velocity.

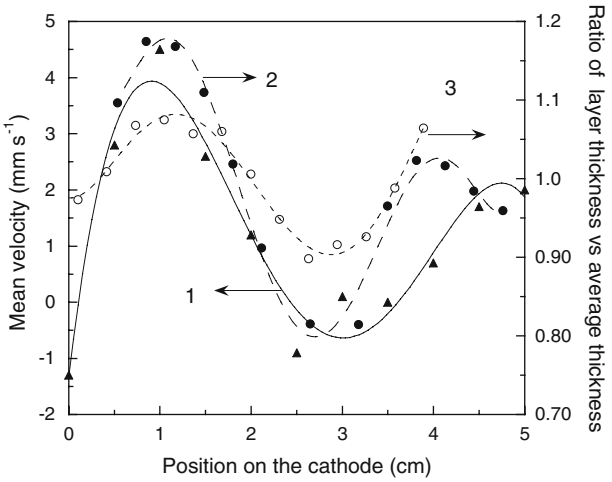


**Fig. 10** Mean velocity distribution (*curve 1*) and relative thickness distribution curves (ratio of local thickness versus average thickness) recorded along the cathode respectively for CIS (*curve 2*) and for Cu–Ni (*curve 3*). (comb speed 104 mm $s^{-1}$, 4 Hz)

## 6 Conclusion

To investigate the hydrodynamic conditions of Cu–In–Se (CIS) alloy electrodeposition processes, a Cu–Ni codeposition system has been examined as a simple model. Polarization behavior and electrodeposition conditions have been determined with a rotating disk electrode, providing significant variations of deposit characteristics (composition and thickness) as a function of electrode rotation speed. An electrolyte with a composition corresponding to a Priscott bath has been chosen. For a potential deposition of −1.6 V/MSE, copper is deposited under mass-transfer control, strongly dependent on local hydrodynamics, whereas nickel is codeposited under charge transfer control (independent of hydrodynamics).

Both the model Cu–Ni and industrial CIS systems have been studied in a small pilot cell with a 5 × 5 $cm^2$ working electrode, with electrolyte agitation provided by a comb-like system. The copper partial current density variations along the cathode for the Cu–Ni system show fluctuations characteristic of a tertiary current distribution, with a strong dependence on local hydrodynamics, whereas the nickel partial current distribution shows a primary distribution, independent of hydrodynamics. Similar variations in partial current density with local hydrodynamics are observed for Cu and Se for the CIS system, with little or no influence of local hydrodynamics on partial current.

The investigation demonstrates that the deposition kinetics of both systems, Cu–Ni and Cu–In–Se, show strong similarities: copper is deposited under mass-transfer control in both systems, nickel and indium content depends mainly on deposition potential, independent of mass-transfer conditions. Measurements in both systems indicate clearly that the thickness distribution of the electro-deposit results from variations in local hydrodynamics.

The experimental comparison confirms that the mass-transfer characteristics measured for copper deposition in the binary Cu–Ni codeposition system offer an excellent representation of the mass-transfer-limited deposition of copper and selenium in the ternary CIS system.

The Cu–Ni system should be particularly useful, as a safe, simple, inexpensive and non-toxic model for scale-up of plating processes and optimization of devices for effective electrolyte agitation.

## References

1. Lincot D, Guillemoles JF, Taunier S, Guimard D, Sicx-Kurdi J, Chomont A, Roussel O, Grand PP, Benfarah M, Mogensen P, Kerrec O (2004) Sol Energy 77:725
2. Taunier S, Sicx-Kurdi J, Grand PP, Chomont A, Ramdani O, Parissi L, Panheleux P, Naghavi N, Hubert C, Ben-Farah M,

Fauvarque JP, Connolly J, Roussel O, Mogensen P, Mahe E, Guillemoles JF, Lincot D, Kerrec O (2005) Thin Solid Films 480:26
3. Delbos S, Grand PP, Fanouillère P, Weitbrecht V, Jirka G, Chassaing E, Lincot D, Kerrec O (2007) 211th Electrochemical Society Meeting: abstract # 888
4. Bhattacharya RN (1983) J Electrochem Soc 130:2040
5. Pottier D, Maurin G (1989) J Applied Electrochem 19:361
6. Mishra K, Rajeshwar K (1989) J Electroanal Chem 271(1–2):279
7. Thouin L, Massaccesi S, Sanchez S, Vedel J (1994) J Electroanal Chem 374(1–2):81
8. Thouin L, Rouquette-Sanchez S, Vedel J (1994) Electrochim Acta 38:2387
9. Menezes S (1996) Mater Res Soc Symp Proc 426:189
10. Oliveira MCF, Azevedo M, Cunha A (2002) Thin Solid Films 405:129
11. Kemell M, Ritala M, Leskela M (2005) Crit Rev Solid State Mater Sci 30(1):1
12. Kois J, Bereznev S, Mellikov E, Opik A (2006) Thin Solid Films 511:420
13. Chassaing E, Roussel O, Ramdani O, Grand PP, Canava B, Etcheberry A, Guillemoles JF, Lincot D (2007) In: SOTAPOCS 46 and Processes at the Semiconductor/Solution Interface 2, The Electrochemical Society 6-Issue 2:577
14. Kröger FA (1978) J Electrochem Soc 125:2028
15. Ramdani O, Guillemoles JF, Lincot D, Grand PP, Chassaing E, Kerrec O, Repka E (2007) Thin Solid Films 515:5909
16. Pourbaix M (1963) Atlas electrochimique. Gauthier-Villars, Paris
17. Landolt D (1994) Electrochim Acta 39:1075
18. Brenner A (1963) Electrodeposition of alloys. Academic Press, New York
19. Priscott BH (1959) Trans Inst Met Finish 36:93
20. Rode S, Henninot C, Vallières C, Matlosz M (2004) J Electrochem Soc 151:C405
21. Rode S, Henninot C, Matlosz M (2005) J Electrochem Soc 152:C248
22. Chassaing E, Vu Quang K, Wiart R (1987) J Applied Electrochem 17:126
23. Ying RA (1988) J Electrochem Soc 135:2957
24. Madore C (1993) Ph.D Dissertation, Ecole Polytechnique Fédérale de Lausanne No. 1189
25. Ibl N (1975) Oberfläche-Surface 16:23